Yu Ding
Dept. of Industrial Engineering,
Texas A&M University,
College Station, TX 77843-3131
e-mail: yuding@email.tamu.edu

Dariusz Ceglarek
Dept. of Industrial Engineering,
University of Wisconsin-Madison,
Madison, WI 53706
e-mail: darek@engr.wisc.edu

Jianjun Shi
Dept. of Industrial and Operations Engineering,
The University of Michigan,
Ann Arbor, MI 48109
e-mail: shihang@umich.edu

Fault Diagnosis of Multistage Manufacturing Processes by Using State Space Approach

This paper presents a methodology for diagnostics of fixture failures in multistage manufacturing processes (MMP). The diagnostic methodology is based on the state-space model of the MMP process, which includes part fixturing layout geometry and sensor location. The state space model of the MMP characterizes the propagation of fixture fault variation along the production stream, and is used to generate a set of predetermined fault variation patterns. Fixture faults are then isolated by using mapping procedure that combines the Principal Component Analysis (PCA) with pattern recognition approach. The fault diagnosability conditions for three levels: (a) within single station, (b) between stations, and (c) for the overall process, are developed. The presented analysis integrates the state space model of the process and matrix perturbation theory to estimate the upper bound for isolationability of fault pattern vectors caused by correlated and uncorrelated noises. A case study illustrates the proposed method. [DOI: 10.1115/1.1445155]

1 Introduction

Dimensional quality, represented by product dimension variability, is one of the most critical challenges in industries which use multistage manufacturing processes such as assembly and machining for automotive, aerospace, or appliance products. The complexity of a manufacturing process puts high demands on process modeling, design optimization, and on fault diagnosis to ensure the dimensional integrity of the product.

In general, part fixturing, which determines the positions of parts during manufacturing (assembly or machining), directly affects the dimensional quality of final products. During the launch of a new automobile, for example, fixture faults accounted for 72 percent of all the dimensional faults [1].

Recent advancements in fixture design have resulted in significant improvement of fixturing accuracy and repeatability [2–4]. Nevertheless, design-oriented methodology alone cannot guarantee the desired quality of the product due to the complexity and random nature of uncertainties and disturbances in manufacturing processes. Therefore, an effective method for detecting and diagnosing dimensional faults during production, based on in-line measurements, is highly desirable.

The aforementioned factors have led to modeling and diagnosis of manufacturing processes to emerge as a new research area lying within the boundary of engineering and statistics research, and has grown rapidly during the last few years. Methodologies proposed include pattern recognition of single fixture fault through Principal Component Analysis (PCA) [5], and the identification of multiple simultaneous faults, using least estimation followed by statistical testing [6,7]. These approaches were also applied to the diagnostics of compliant assembly processes [8,9]. These diagnostics require the pattern vectors to be obtained through off-line modeling ($\mathbf{d}(i)$'s in [5], $\mathbf{a}_i$'s in [6], and $\mathbf{c}_i$'s in [7]). Such pattern vectors are relatively easy to obtain for a fixture fault on a single manufacturing station, and is the case discussed in the above mentioned papers.

The modeling of pattern vectors for all potential fixturing faults in a multistage manufacturing process (MMP) is much more challenging due to the complex interrelations that exist between stations, thus causing, for example, fixture fault patterns resulting from operations at upstream stations that can be affected by downstream operations. Further, the transfer of a part and/or intermediate product between stations may introduce variation not include by single station modeling. Thus, it is insufficient to generate fault pattern vectors for an MMP by simply grouping together the pattern vectors obtained separately from individual stations. Rather a process-level model is required to characterize such propagation and accumulation of variation, and to relate the fixture variation to the dimension quality of the final product. Such process-level models did not exist until recently [10–13]. Among these proposed models, tooling variation, including fixture variation, is only explicitly considered by Jin and Shi [13], where a state space modeling approach is used to recursively describe variation propagation at the process level of a multistage process.

The state space model is a different form of the standard kinematic analysis model, also utilized in such software as Variation Simulation Analysis [14], which is widely used and commercially available. The state space model provides analytical tools for system evaluation and synthesis thus going beyond numerical simulation; the commercial software is mostly based on pure numerical analysis and trial-and-error synthesis approach. Although Jin and Shi [13] presented expressions for model parametric matrices only for simplified assembly processes, the modeling framework is fairly general and can be extended to more complex situations in assembly, and also to other manufacturing processes such as the machining process [15]. Thus, we think that a state space model can be a good modeling framework for fixture fault diagnosis in MMPs.

This paper proposes a diagnostic approach for diagnosing fixture faults in a given MMP system. A systematic method of modeling variation propagation and fault pattern vectors is developed by using the state space model. A PCA-based algorithm similar to the one proposed in [5] is employed for single fault diagnosis. Analytical upper bounds of the perturbation in pattern vectors due to the correlated noise are found using matrix perturbation theory. Although certain assumptions imposed in the current paper helped to set up a complete approach for the fixture diagnostics of MMPs, neither the framework of the state space modeling nor the diagnostics approach is bound by these assumptions. Thus, we think that the proposed diagnostic method provides a better understanding of the process and creates analytical foundation for further optimization and control of MMP systems.

This paper is divided into five sections. Section 2 derives a variation propagation model from the state space model of an MMP. Section 3 presents the diagnostic method for the single

Contributed by the Manufacturing Engineering Division for publication in the JOURNAL OF MANUFACTURING SCIENCE AND ENGINEERING. Manuscript received Nov. 1999; Revised March 2001. Associate Editor: R. Furness.

fault situation in an MMP, followed by the perturbation analysis. In Section 4, fault patterns of an assembly process are first generated and then interpreted. Computer simulation is used to illustrated and verify the proposed method. Finally, this work is summarized in Section 5.

2 Variation Propagation Model

The variation propagation model, which will be used for diagnostic methods is based on the model developed by Jin and Shi [13]. The propagation of deviation in an *m*-station MMP can be represented in the form of state space equations

$$\mathbf{X}(i)=\mathbf{A}(i-1)\mathbf{X}(i-1)+\mathbf{B}(i)\mathbf{U}(i)+\mathbf{V}(i), \quad i\in[1,2,\ldots,m] \tag{1}$$

$$\mathbf{Y}(i)=\mathbf{C}(i)\mathbf{X}(i)+\mathbf{W}(i), \quad \{i\}\subset\{1,2,\ldots,m\} \tag{2}$$

where $\mathbf{A}(i-1)$ corresponds to the term $\mathbf{I}+\mathbf{T}(i-1)$ in Eq. (36) in [13]. The state space model is extended from its previous version [13] to accommodate more general manufacturing processes. The difference is briefly discussed in Appendix II.

In Eqs. (1) and (2), **X** represents the part deviation at station *i*, **U** is the fixturing deviation contributed from station *i*, and **Y** is the deviation vector containing all measurements at the Key Product Characteristics (KPC) points. **V** and **W** are process noise such as background disturbance and unmodeled error, and sensor noise, respectively. **V** and **W** are assumed to be mutually independent. These definitions follow the same notation as used in [13]. Matrices **A, B**, and **C** encode the design information of process configuration. **A** is the dynamic matrix, determined by the deviation change due to part transfer among stations. **B** is the input matrix, depending on the fixture layout at each station. **C** is the observation matrix, corresponding to the information of the sensor number and locations.

Equation (1), known as the state equation, implies that the part deviation at station *i* is influenced by two sources: the accumulated part deviation up to station $i-1$, and the deviation contributed at the current station. Equation (2) is the observation equation. If sensors are installed at one or more stations in a production line, the index for the observation equation is actually a subset of $\{1,2,\ldots m\}$, whereas the index for the state equation is the complete set.

This paper employs the end-of-line sensing strategy, which is the most commonly used sensor installation scheme in industry. End-of-line sensing means that observation is only available at the last station *m*, that is, $i=m$ for Eq. (2), and

$$\mathbf{Y}=\mathbf{C}\mathbf{X}(m)+\mathbf{W} \tag{3}$$

where $\mathbf{Y}\in\mathbf{R}^{k\times 1}$ indicates the *k* measurements are obtained at station *m*. The indices for **Y**, **C**, and **W** are dropped since they are all '*m*'s.

State transition matrix $\mathbf{\Phi}(\cdot,\cdot)$ is adopted from linear control theory [16] and is defined as

$$\mathbf{\Phi}(m,i)=\mathbf{A}(m-1)\mathbf{A}(m-2)\cdots\mathbf{A}(i) \text{ for } m>i \text{ and } \mathbf{\Phi}(i,i)=\mathbf{I}. \tag{4}$$

The input-output relationship can then be represented as

$$\mathbf{Y}=\sum_{i=1}^{m}\mathbf{C}\mathbf{\Phi}(m,i)\mathbf{B}(i)\mathbf{U}(i)+\mathbf{C}\mathbf{\Phi}(m,0)\mathbf{X}(0)+\boldsymbol{\varepsilon}, \tag{5}$$

where $\mathbf{X}(0)$ corresponds to the initial condition (for instance, the fabrication imperfection of product components in an assembly) and $\boldsymbol{\varepsilon}$ is the summation of all modeling uncertainty and sensor noise terms, where

$$\boldsymbol{\varepsilon}=\sum_{i=1}^{m}\mathbf{C}\mathbf{\Phi}(m,i)\mathbf{V}(i)+\mathbf{W}. \tag{6}$$

Define $\boldsymbol{\gamma}(i)$ and $\boldsymbol{\gamma}(0)$ as

$$\boldsymbol{\gamma}(i)=\mathbf{C}\mathbf{\Phi}(m,i)\mathbf{B}(i) \text{ and } \boldsymbol{\gamma}(0)=\mathbf{C}\mathbf{\Phi}(m,0). \tag{7}$$

where *m* is dropped from the indices of $\boldsymbol{\gamma}$ for this end-of-line sensing scheme. Then, Eq. (5) can be simplified as

$$\mathbf{Y}=\sum_{i=1}^{m}\boldsymbol{\gamma}(i)\mathbf{U}(i)+\boldsymbol{\gamma}(0)\mathbf{X}(0)+\boldsymbol{\varepsilon} \tag{8}$$

Here, $\mathbf{X}(0)$, $\mathbf{W}$, $\mathbf{V}_{i=1}^{m}(i)$ are the basic random variables in a stochastic process and thus usually assumed to be independent. The assumption can be partially released to include the situation where the basic random variables are dependent by enlarging the state vector [17]. Moreover, $\mathbf{U}_{i=1}^{m}(i)$, the fixturing deviations at station *i*, are independent with those basic random variables as well since only an open loop system is considered now. Given the independent relationships between these variables, the input-output covariance relationship could be obtained from Eq. (8) to characterize the variation propagation in a production line,

$$\mathbf{K}_Y=\sum_{i=1}^{m}\boldsymbol{\gamma}(i)\mathbf{K}_U(i)\boldsymbol{\gamma}^T(i)+\boldsymbol{\gamma}(0)\mathbf{K}_0\boldsymbol{\gamma}^T(0)+\mathbf{K}_\varepsilon, \tag{9}$$

where $\mathbf{K}_Y$ represents the covariance matrix of random vector **Y**, and $\mathbf{K}_0$ is given as the initial variability condition. $\mathbf{K}_\varepsilon$ can be estimated from the data during which no fixture fault was present.

Jin and Shi [13] assumed that only the lap joint is involved in the current model, implying that the fabrication imperfection of parts will not affect the propagation of variations. Thus, it is reasonable to set the initial condition $\mathbf{K}_0$ to zero. The process can then be approximated as follows:

$$\mathbf{K}_Y=\sum_{i=1}^{m}\boldsymbol{\gamma}(i)\mathbf{K}_U(i)\boldsymbol{\gamma}^T(i)+\mathbf{K}_\varepsilon. \tag{10}$$

This equation suggests that, while being contaminated by noise, the variation of the final product is mainly the contribution of variations of fixturing errors at all stations.

3 Diagnosis of Fixture Fault in MMPs

3.1 The Overall Concept. The overall concept of the diagnostic methodology is shown in Fig. 1. If a fixturing element (locator) does not function properly, a symptom will be reflected in the final product or downstream intermediate products. From off-line CAD information and the created earlier state space model, the set of all possible fault patterns can be generated. Measurement data are collected in-line and analyzed using one of the multivariate statistical methods, for example, the Principal Component Analysis [18], to extract the fault feature patterns. Fault isolation can then be conducted by mapping the feature patterns of real production data with the pre-determined fault patterns generated from the analytical model.

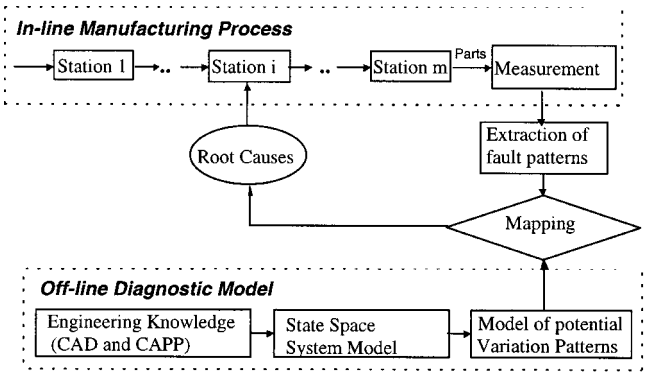

Fig. 1 Outline of the diagnostic methodology

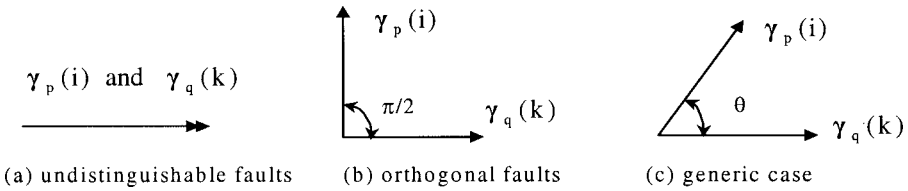

Fig. 2 Angle between two fault patterns

For the sake of simplicity and better illustration, the diagnostic methodology for the MMP systems is presented in the context of automotive body assembly process. However, the proposed approach and analysis are not limited to a specific automotive manufacturing process. The presented methodology can be used for a class of MMPs which can be modeled by using the state space framework.

3.2 Single Fault Patterns Without Noise Consideration. A detailed description of an autobody assembly process can be found in [19]. Suppose there are n_i subassemblies on each station in an m-station assembly process. Each of the subassemblies is supported by the 3-2-1 fixture layout, which consists of a pair of locating pins $P_{4\text{way}}$ and $P_{2\text{way}}$ and three NC blocks. An illustrative picture is included in Appendix I for reference. Due to the modeling assumption used in [13], the currently developed state space model only includes the fixturing deviation from the 4-way and 2-way locating pins. Each of the pins could be faulty in two orthogonal dimensions. A simple calculation reveals that the number of potential single faults in the process is $\Sigma_{i=1}^{m} 4n_i$.

Let p be the index of fixture (locating pin) fault at the ith station, which could be one of the $4n_i$ potential single faults ($p=1,2,\ldots,4n_i$). Assuming that all pin deviations at station i are uncorrelated with each other, $\mathbf{K}_U(i)$ is a diagonal matrix. When only fault p occurs at station i, matrix $\mathbf{K}_U(i)$ appears as follows:

$$\mathbf{K}_U(i)=\begin{bmatrix} 0 & & & \\ & \ddots & & \\ & & \sigma_p^2 & \\ & & & \ddots \\ & & & & 0 \end{bmatrix} \tag{11}$$

where only the (p, p) entry is a non-zero value σ_p^2, the variance of the fault. The pattern vectors of potential fixture faults are first obtained without considering the noise term, $\mathbf{K}_\varepsilon$, i.e. from the covariance matrix $\mathbf{K}_Y^0$, which is not contaminated by noise. $\mathbf{K}_Y^0$ is obtained by substituting Eq. (11) into Eq. (10) and dropping the term $\mathbf{K}_\varepsilon$ to yield

$$\mathbf{K}_Y^0=\sigma_p^2\boldsymbol{\gamma}_p(i)\boldsymbol{\gamma}_p^T(i), \tag{12}$$

where the superscript T denotes vector transpose and $\boldsymbol{\gamma}_p(i)$ is the pth column of matrix $\boldsymbol{\gamma}(i)$. Equation (12) implies that the rank of $\mathbf{K}_Y^0$ is one, that is, one eigenvalue is non-zero and all others are zero. It is also known that $\boldsymbol{\gamma}_p(i)$ is the eigenvector corresponding to the only non-zero eigenvalue λ_{ip} (fault p at station i), that is,

$$\mathbf{K}_Y^0\boldsymbol{\gamma}_p(i)=\lambda_{ip}\boldsymbol{\gamma}_p(i) \tag{13}$$

resulting in

$$\boldsymbol{\gamma}_p(i)\{\sigma_p^2\boldsymbol{\gamma}_p^T(i)\boldsymbol{\gamma}_p(i)-\lambda_{ip}\}=\mathbf{0} \tag{14}$$

which indicates,

$$\lambda_{ip}=\sigma_p^2\boldsymbol{\gamma}_p^T(i)\boldsymbol{\gamma}_p(i)=\|\sigma_p\boldsymbol{\gamma}_p\|_2^2 \tag{15}$$

where $\|\cdot\|_2$ is the Euclidean norm. The eigenvalue λ_{ip} represents the variance of the principal component. In a single fault situation, it indicates the variation level of a product. The eigenvector is the pattern vector of a fixture fault, manifesting the fixturing variation by generating a mode shape of measurement vector $\mathbf{Y}$. If one repeats this for the entire range of single fault candidates, the eigenvalue-eigenvector pairs $\{\lambda_{ip}, \boldsymbol{\gamma}_p(i)\}$ will constitute the set of candidate fixture fault patterns. In the rest of this paper, assume $\boldsymbol{\gamma}_p(i)$ as a normalized eigenvector using the Euclidean norm.

3.3 Fault Isolation and Diagnosability With the Presence of Noise. Given any two fault patterns $\boldsymbol{\gamma}_p(i)$ and $\boldsymbol{\gamma}_q(k)$, which are the symptoms of fault p at station i and fault q at station k, respectively, the similarity between the two faults can be expressed in the acute angle formed by fault pattern vectors,

$$\theta_{pq}(i,k)=\cos^{-1}\langle\boldsymbol{\gamma}_p(i),\boldsymbol{\gamma}_q(k)\rangle,\quad 0\leqslant\theta\leqslant\frac{\pi}{2}, \tag{16}$$

where $\langle\cdot,\cdot\rangle$ represents the inner product of two vectors. Consider two special cases, $\theta=0$ and $\theta=\pi/2$.

If $\theta=0$, the two vectors are collinear. The fault patterns are identical and, therefore, the corresponding faults are undistinguishable in this case (Fig. 2(*a*)).

If $\theta=\pi/2$, the two vectors are perpendicular to each other. In this situation, the two faults are called orthogonal. It is obvious that orthogonal faults ensure maximum diagnosability (Fig. 2(*b*)).

If θ has a value between 0 and $\pi/2$, as long as θ is not zero, the two faults are distinct (Fig. 2(*c*)). However, small θ implies that two fault patterns are close to each other. Under the influence of noise, fault patterns might be undistinguishable. Thus, the larger θ is, the easier are the faults that can be distinguished.

With the presence of noise,

$$\mathbf{K}_Y=\mathbf{K}_Y^0+\mathbf{K}_\varepsilon. \tag{17}$$

Denote the eigenvalue and eigenvector of $\mathbf{K}_Y$ as $\{\lambda, \boldsymbol{\gamma}\}$ and those of $\mathbf{K}_Y^0$ as $\{\lambda^0, \boldsymbol{\gamma}^0\}$. The pattern vectors obtained from Eq. (12) are actually $\boldsymbol{\gamma}^0$'s. The difference between $\boldsymbol{\gamma}$ and $\boldsymbol{\gamma}^0$ due to the additive noise $\mathbf{K}_\varepsilon$ is studied by Ceglarek and Shi [20] for the case where $\mathbf{K}_\varepsilon$ is diagonal. Although this is a reasonable assumption in a single station case, it is not valid for an MMP. Consider Eq. (6). Even if all $\mathbf{V}$'s are assumed mutually independent, elements in $\boldsymbol{\varepsilon}$ may be correlated in general after being filtered by $\mathbf{C\Phi}(m,i)$. In fact, the evaluation of pattern perturbation under the influence of *correlated noise* may not be adequately handled by the diagnostic algorithms proposed for the single station situation, which are usually employed for cases of *uncorrelated* noise.

Matrix perturbation theory [21] is employed to evaluate the upper bound on the perturbation of pattern vectors due to the influence of correlated noise. Theorem 8.1.12 in [21] derives an upper bound of eigenvector perturbation for a symmetric matrix $\mathbf{S}$ under the influence of another symmetric perturbation matrix $\mathbf{E}$. This theorem is stated in Appendix III for the reader's reference.

Since the covariance matrix $\mathbf{K}$ is always symmetric, the results of this theorem apply here. Noting that $\mathbf{K}_Y^0$ only has one non-zero eigenvalue λ^0, therefore, there exists an orthogonal matrix $\mathbf{Q}=[\boldsymbol{\gamma}^0\ \ \mathbf{Q}_2]$ such that

$$\mathbf{Q}^T\mathbf{K}_Y^0\mathbf{Q}=\begin{bmatrix}\lambda^0 & \mathbf{0}\\ \mathbf{0} & \mathbf{0}\end{bmatrix}\ \text{ and }\ \mathbf{Q}^T\mathbf{K}_\varepsilon\mathbf{Q}=\begin{bmatrix}(\boldsymbol{\gamma}^0)^T\mathbf{K}_\varepsilon\boldsymbol{\gamma}^0 & (\boldsymbol{\gamma}^0)^T\mathbf{K}_\varepsilon\mathbf{Q}_2\\ \mathbf{Q}_2^T\mathbf{K}_\varepsilon\boldsymbol{\gamma}^0 & \mathbf{Q}_2^T\mathbf{K}_\varepsilon\mathbf{Q}_2\end{bmatrix}. \tag{18}$$

Following the definition for d in Theorem 8.1.12, we may conclude that $d=\lambda^0>0$. Furthermore, if the condition $\|\mathbf{K}_\varepsilon\|_2\leqslant\lambda^0/4$ is also satisfied, the upper bound of the angle between $\boldsymbol{\gamma}^0$ and $\boldsymbol{\gamma}$ is

$$\Delta\theta\leqslant\sin^{-1}\left(\frac{4}{\lambda^0}\sqrt{\|\mathbf{K}_\varepsilon\boldsymbol{\gamma}^0\|_2^2-(\boldsymbol{\gamma}^{0T}\mathbf{K}_\varepsilon\boldsymbol{\gamma}^0)^2}\right)$$

$$\leqslant\sin^{-1}\left(\frac{4}{\lambda^0}\sqrt{\lambda_{\max}^2(\mathbf{K}_\varepsilon)-\lambda_{\min}^2(\mathbf{K}_\varepsilon)}\right), \tag{19}$$

where $\lambda(\cdot)$ is the eigenvalue of a matrix. The proof of this result is presented in Appendix IV.

Remark 1. The condition $\|\mathbf{K}_\varepsilon\|_2\leqslant\lambda^0/4$ required for Eq. (19) is not restrictive in practice. Notice that $\|\mathbf{K}_\varepsilon\|_2=\lambda_{\max}(\mathbf{K}_\varepsilon)$ is the largest variance of noise, and λ^0 is the variance of a fixture fault, $\lambda_{\max}(\mathbf{K}_\varepsilon)\leqslant\lambda^0/4$, suggesting that the standard deviation of noise is less than one half of the standard deviation of a fixture fault. This condition is usually satisfied. If the noise in the MMP is severer than this level, the eigenvector will be distorted to the point where this PCA-based recognition approach will no longer be effective.

Remark 2. There are two upper bounds given in Eq. (19), that is

$$b_1(\boldsymbol{\gamma}^0)=\sin^{-1}\left(\frac{4}{\lambda^0}\sqrt{\|\mathbf{K}_\varepsilon\boldsymbol{\gamma}^0\|_2^2-(\boldsymbol{\gamma}^{0T}\mathbf{K}_\varepsilon\boldsymbol{\gamma}^0)^2}\right)\quad\text{and}$$

$$b_2=\sin^{-1}\left(\frac{4}{\lambda^0}\sqrt{\lambda_{\max}^2(\mathbf{K}_\varepsilon)-\lambda_{\min}^2(\mathbf{K}_\varepsilon)}\right).$$

The bound b_1 is different for individual eigenvectors and preferred since it is tighter than b_2. However, it requires $\mathbf{K}_\varepsilon$ to be known or estimable. The bound b_2 only requires the knowledge of the extreme eigenvalues of $\mathbf{K}_\varepsilon$, which may be more easily estimated from production data. For instance, Apley and Shi [22] estimated the variance of noise (equivalent to the eigenvalue of $\mathbf{K}_\varepsilon$) from $\mathbf{K}_Y$. The tightness of b_2 depends on the difference between the extreme eigenvalues of $\mathbf{K}_\varepsilon$. Since the noise normally exists in process uniformly and any outstanding deviation away from the nominal is grouped into the term $\mathbf{K}_Y^0$ as fault condition, $\mathbf{K}_\varepsilon$ is fairly well-posed. Thus, the recognition result will not be very conservative when b_2 is used.

Remark 3. According to the upper bound b_2, it is not the variance of noise associated with each measurement point but their difference $(\lambda_{\max}^2(\mathbf{K}_\varepsilon)-\lambda_{\min}^2(\mathbf{K}_\varepsilon))$ that accounts for the distortion in fault pattern vectors. If $\mathbf{K}_\varepsilon=\sigma_\varepsilon^2\mathbf{I}$, i.e., the noises are uncorrelated and have the same variances for all KPCs, then $b_2=0$, meaning that the fault pattern vectors will not be altered. The above conclusions are consistent with those presented in [20] for a single-station manufacturing process. But the bounds b_1 and b_2 provide general analytical expression for the robustness evaluation of the PCA-based approach in pattern recognition.

By using the upper bounds, conditions for the diagnosability of an individual station, between stations, and of the entire process are presented here on the single fault assumption.

(1) Diagnosability within an individual station

If it is known on which station a fault occurred, the question is then under what condition we can tell which fixture (locator or clamp) on the specific station causes the fault. Given that the fault patterns at station i are represented by the column vectors of matrix $\boldsymbol{\gamma}(i)$, the smallest angle between any two pattern vectors p and q at station i can be defined as

$$\theta_{\min}(i)=\min_{p,q}\theta_{pq}(i,i) \tag{20}$$

Then, a single fixture fault on station i can be diagnosed if and only if

$$\theta_{\min}(i)>2b_2 \tag{21}$$

If $b_1(\boldsymbol{\gamma}_p(i))$'s are known, the following condition will be less conservative

$$\min_{p,q}\{\theta_{pq}(i,i)-2b_1(\boldsymbol{\gamma}_p(i))\vee 2b_1(\boldsymbol{\gamma}_q(i))\}>0 \tag{22}$$

where $a\vee b\equiv\max(a,b)$ for any real number a and b.

(2) Diagnosability between stations

The second scenario asks whether we could tell on which station the fault occurred based on the end-of-line measurement. With the fault pattern angle between station i and station k defined as

$$\theta(i,k)=\min_{p,q}\theta_{p,q}(i,k), \tag{23}$$

the between-station diagnosability is ensured if and only if

$$\min_{\substack{i,k\\ i\neq k}}\theta(i,k)>2b_2\quad\text{or}$$

$$\min_{\substack{i,k\\ i\neq k}}\min_{p,q}\{\theta_{pq}(i,k)-2b_1(\boldsymbol{\gamma}_p(i))\vee 2b_1(\boldsymbol{\gamma}_q(k))\}>0. \tag{24}$$

(3) Diagnosability of the entire process

If the above two conditions are satisfied, the fixture fault can first be localized at a certain station and then identified right on that station. Diagnosability of the entire process is equivalent to the combination of two previous equations, (21) and (24):

$$\min_{i,k}\theta(i,k)>2b_2\quad\text{or}$$

$$\min_{i,k}\min_{p,q}\{\theta_{pq}(i,k)-2b_1(\boldsymbol{\gamma}_p(i))\vee 2b_1(\boldsymbol{\gamma}_q(k))\}>0. \tag{25}$$

4 A Case Study

4.1 Single-Fault Patterns and Geometric Interpretation. In this section, a multistage assembly process is set up. This process is abstracted from a side aperture assembly line in the automotive industry, including three assembly stations and one measurement station. The final product is made of four parts, as shown in Fig. 3.

The assembly sequence and datum shift scheme regarding this assembly process are shown in Fig. 4. $\{\{P_1,P_2\},\{P_3,P_4\}\}$ denotes the locating pairs used at station 1, where $\{P_1,P_2\}$ is for the first workpiece and $\{P_3,P_4\}$ for the second one. The others are similarly defined. At station 4, which is the measurement station, one pair of locating pins $\{P_1,P_8\}$ is used since there is only one piece of the assembly to measure.

In the fixture layout indicated in Fig. 3(*b*), a 4-way pin (one of P_1, P_3, P_5, and P_7) controls part motion in both X and Z directions and a 2-way pin (one of P_2, P_4, P_6, and P_8) controls part motion only in the Z direction. It is also assumed that the locating pins at the measurement station are much more accurate than those at assembly stations, which implies that fixture error at the measurement station can be neglected. Hence, the total number of all single fault patterns is $n_f=\Sigma_{i=1}^3(4n_i-2)=18$ with $n_i=2$ for $i=1$, 2, and 3. The relationship between fault indices and root causes on each station is shown in Table 1.

As indicated in Fig. 3(*b*), there are two sensors on each part at the last station (end-of-line sensing). Each sensor can measure part deviation in both X and Z directions. Two sensors are sufficient to detect the deviation in position and orientation of a 2-D rigid part.

Following the derivation of the previous sections, a state space model can be set up for this side aperture assembly process as

$$\begin{cases}\mathbf{X}(1)=\mathbf{B}(1)\mathbf{U}(1)+\mathbf{V}(1)\\ \mathbf{X}(i)=\mathbf{A}(i-1)\mathbf{X}(i-1)+\mathbf{B}(i)\mathbf{U}(i)+\mathbf{V}(i),\quad i=2,3\\ \mathbf{X}(4)=\mathbf{A}(3)\mathbf{X}(3)+\mathbf{V}(4)\\ \mathbf{Y}=\mathbf{C}\mathbf{X}(4)+\mathbf{W}\end{cases} \tag{26}$$

where **A**'s, **B**'s, and **C** can be obtained through Eqs. (38), (39), and (45) in [13].

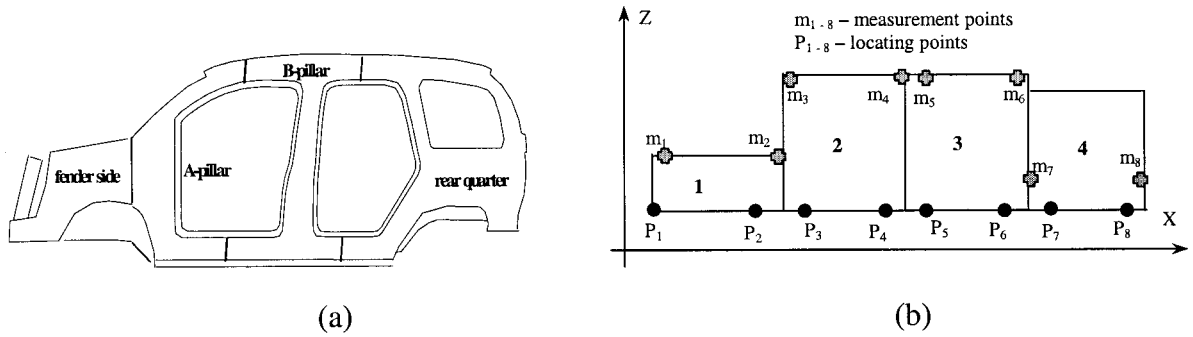

Fig. 3 Geometry of the assembly

Based on this state space model, matrix $\boldsymbol{\gamma}(i)$ is equal to $\mathbf{CA}(3)\cdots\mathbf{A}(i)\mathbf{B}(i)$ by substituting the state transition matrix $\boldsymbol{\Phi}$ into Eq. (7). Then the total of 18 potential single fault patterns can be generated from the column vectors of $\boldsymbol{\gamma}_{i=1}^{3}(i)$. The fault patterns are shown in Table 2(*a*), (*b*), and (*c*), where L_{ij} represents the distance between pin P_i and pin P_j, that is, $L_{ij}=\sqrt{(X_{p_i}-X_{p_j})^2+(Z_{p_i}-Z_{p_j})^2}$, and ΔX_i, ΔZ_i, and $\Delta\alpha_i$ represent the deviation in position and orientation of each part. Because the pattern vectors listed in Table 2(*a*), (*b*), and (*c*) are not normalization, in order to be consistent with the current algorithm, normalization should be conducted before doing any numerical calculation.

The fault patterns in Table 2(*a*), (*b*), and (*c*) have a clear geometric interpretation. For example, if the 4-way pin at the first subassembly is faulty in the Z direction at the second station, that is $p=2$ and $i=2$, then

$$\boldsymbol{\gamma}_2(2)=\left[0\ \ 0\ \ \frac{L_{14}-L_{16}}{L_{13}L_{14}}\ \vdots\ 0\ \ \frac{L_{14}-L_{16}}{L_{14}}\ \ \frac{L_{14}-L_{16}}{L_{13}L_{14}}\ \vdots\ 0\ \ \frac{-L_{56}}{L_{13}}\ \ \frac{1}{L_{13}}\ \vdots\ 0\ \ 0\ \ 0\right]^T. \tag{27}$$

The counter-clockwise is the positive rotation direction as defined in [13]. Thus, $\Delta\alpha_1=\Delta\alpha_2<0$ suggests that part 1 and part 2 rotated the same amount in a clockwise direction. This can be justified because part 1 and part 2 have already been welded together in the previous station, thus behaving as one rigid part. Since P_1 is free of deviation at the measurement station, ΔX_1 and ΔZ_1 are always zeros. The fact that ΔZ_2 is less than zero is consistent with the part rotation. $\Delta\alpha_3>0$ implies that part 3 rotates in the counter-clockwise direction. This seems counterintuitive, because part 3 should not have a deviation at the 2nd station if there only exists one fixture fault. However, the new subassembly "1+2+3" has a reorientation-induced deviation at the 3rd station, where it appears that part 3 rotates relative to subassembly "1+2" in the counter-clockwise direction (Fig. 5). Part 4 is not affected by fault $p=2$ at station 2 since it has not yet come into the stream of assembly.

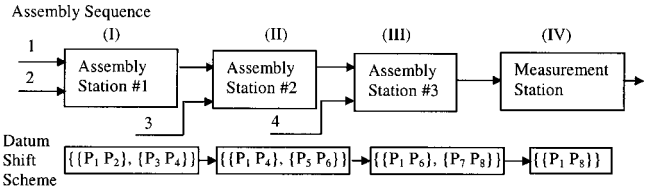

Fig. 4 Assembly sequence and datum shift scheme

All six fault manifestations at the 1st station are listed in Table 3. The fault manifestations at the 2nd and 3rd stations look very similar except that the first subassembly consists of more than one part. However, they behave like one rigid part in the single fault situation.

Consider the satisfaction of diagnosability conditions of this process using Eqs. (21)–(25). At every station, the patterns of faults $p=1$ and $p=4$ are identical, and thus $\theta_{\min}(i,i)_{i=1,2,3}=0$. As a result, the conditions in Eqs. (21) and (22) are both invalidated, meaning that the single fixture fault cannot be completely diagnosed on each station. No matter which pin is faulty in X direction, the symptom is only reflected in the deviation of the second part or subassembly. Only the relative deviation between two parts in the X direction can be detected.

However, faults $p=1$ (or 4) and $p=2$, 3, 5, and 6, on the other hand, have distinct fault patterns within each station. There is no identical between-station fault pattern found among the three stations. But whether these non-identical fixture faults are guaranteed distinguishable depends on the noise level, i.e. bounds b_1 or b_2.

Table 1 Fault indices and their root causes

Index	Fault root cause	Index	Fault root cause
p=1	4-way pin on the 1st part/subassembly is faulty in X direction	p=4	4-way pin on the 2nd part/subassembly is faulty in X direction
p=2	4-way pin on the 1st part/subassembly is faulty in Z direction	p=5	4-way pin on the 2nd part/subassembly is faulty in Z direction
p=3	2-way pin on the 1st part/subassembly is faulty in Z direction	p=6	2-way pin on the 2nd part/subassembly is faulty in Z direction

Table 2 (*a*) Pattern vectors of single fault for the 1st station

element \ vector		$\gamma_1(1)$ p=1	$\gamma_2(1)$ p=2	$\gamma_3(1)$ p=3	$\gamma_4(1)$ p=4	$\gamma_5(1)$ p=5	$\gamma_6(1)$ p=6
1	ΔX_1	0	0	0	0	0	0
2	ΔZ_1	0	0	0	0	0	0
3	$\Delta\alpha_1$	0	$\frac{L_{14}-L_{12}}{L_{12}L_{34}}$	1	0	0	$\frac{1}{L_{13}}$
4	ΔX_2	1	0	0	1	0	0
5	ΔZ_2	0	1	0	0	1	1
6	$\Delta\alpha_2$	0	$-\frac{1}{L_{34}}$	0	0	$-\frac{1}{L_{34}}$	$-\frac{1}{L_{34}}$
7	ΔX_3	0	0	0	0	0	0
8	ΔZ_3	0	0	0	0	0	0
9	$\Delta\alpha_3$	0	0	0	0	0	0
10	ΔX_4	0	0	0	0	0	0
11	ΔZ_4	0	0	0	0	0	0
12	$\Delta\alpha_4$	0	0	0	0	0	0

Table 2 (*b*) Pattern vectors of single fault for the 2nd station

element \ vector		$\gamma_1(2)$ p=1	$\gamma_2(2)$ p=2	$\gamma_3(2)$ p=3	$\gamma_4(2)$ p=4	$\gamma_5(2)$ p=5	$\gamma_6(2)$ p=6
1	ΔX_1	0	0	0	0	0	0
2	ΔZ_1	0	0	0	0	0	0
3	$\Delta\alpha_1$	0	$\frac{L_{14}-L_{16}}{L_{13}L_{14}}$	$\frac{1}{L_{13}}$	0	0	$\frac{1}{L_{13}}$
4	ΔX_2	0	0	0	0	0	0
5	ΔZ_2	0	$\frac{L_{14}-L_{16}}{L_{14}}$	1	0	0	1
6	$\Delta\alpha_2$	0	$\frac{L_{14}-L_{16}}{L_{13}L_{14}}$	$\frac{1}{L_{13}}$	0	0	$\frac{1}{L_{13}}$
7	ΔX_3	1	0	0	1	0	0
8	ΔZ_3	0	$-\frac{L_{56}}{L_{13}}$	0	0	1	$\frac{L_{15}}{L_{13}}$
9	$\Delta\alpha_3$	0	$\frac{1}{L_{13}}$	0	0	$-\frac{1}{L_{56}}$	$-\frac{L_{15}}{L_{13}L_{56}}$
10	ΔX_4	0	0	0	0	0	0
11	ΔZ_4	0	0	0	0	0	0
12	$\Delta\alpha_4$	0	0	0	0	0	0

Table 2 (*c*) Pattern vectors of single fault for the 3rd station

element \ vector		$\gamma_1(3)$ p=1	$\gamma_2(3)$ p=2	$\gamma_3(3)$ p=3	$\gamma_4(3)$ p=4	$\gamma_5(3)$ p=5	$\gamma_6(3)$ p=6
1	ΔX_1	0	0	0	0	0	0
2	ΔZ_1	0	0	0	0	0	0
3	$\Delta\alpha_1$	0	$\frac{L_{16}-L_{18}}{L_{13}L_{16}}$	$\frac{1}{L_{13}}$	0	0	$\frac{1}{L_{13}}$
4	ΔX_2	0	0	0	0	0	0
5	ΔZ_2	0	$\frac{L_{16}-L_{18}}{L_{16}}$	1	0	0	1
6	$\Delta\alpha_2$	0	$\frac{L_{16}-L_{18}}{L_{13}L_{16}}$	$\frac{1}{L_{13}}$	0	0	$\frac{1}{L_{13}}$
7	ΔX_3	0	0	0	0	0	0
8	ΔZ_3	0	$\frac{(L_{16}-L_{18})L_{15}}{L_{13}L_{16}}$	$\frac{L_{15}}{L_{13}}$	0	0	$\frac{L_{15}}{L_{13}}$
9	$\Delta\alpha_3$	0	$\frac{L_{16}-L_{18}}{L_{13}L_{16}}$	$\frac{1}{L_{13}}$	0	0	$\frac{1}{L_{13}}$
10	ΔX_4	1	0	0	1	0	0
11	ΔZ_4	0	$-\frac{L_{78}}{L_{13}}$	0	0	1	$\frac{L_{17}}{L_{13}}$
12	$\Delta\alpha_4$	0	$\frac{1}{L_{13}}$	0	0	$-\frac{1}{L_{78}}$	$\frac{L_{78}-L_{18}}{L_{13}L_{78}}$

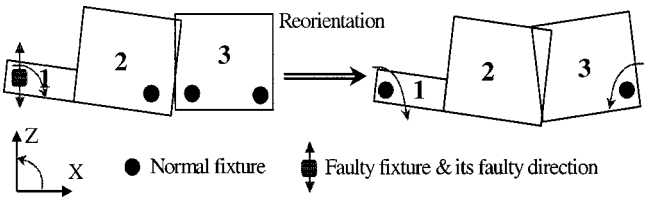

Fig. 5 Geometric interpretation of fault p=2 at the 2nd station

This is discussed further in the following section on the numerical simulation.

It is obvious that diagnosability of the entire process is not ensured since there are identical fault patterns within individual stations. In order to obtain the process diagnosability, extra sensors have to be added directly on the assembly stations.

4.2 Simulations. Although a full diagnosability of the entire process is not ensured with the current sensor installation scheme, faults of $p=2$, 3, 5, 6 do have distinct patterns, which could be correctly identified when one of them occurs. In reality, the correct identification of a fixture fault in the set of $\{p=2,3,5,6\}$ also depends on the severity of the perturbation due to noise. During this simulation study, one of the faults $\{p=2,3,5,6\}$ will be assigned, together with noise and process disturbance, to the assembly process discussed in Section 4.1. The developed technique is used to analyze the data and isolate the faulty fixture.

Before simulation, the CAD information was assigned to the assembly process in Fig. 3. The coordinates of locating and sensing points are listed in Table 4 and 5, respectively.

During simulation, two kinds of additive noises were included, process noise $\mathbf{V}_{i=1}^{m}(i)$ and sensor noise $\mathbf{W}$, and these were assumed to be normally distributed. The severity of both noise sources is defined as

$$N_p=\frac{\sigma_V}{\sigma_f} \text{ and } N_m=\frac{\sigma_W}{\sigma_f}, \tag{28}$$

where σ_f is the standard deviation of faulty fixture, σ_V and σ_W are the standard deviations of each element in $\mathbf{V}_{i=1}^{m}(i)$ and $\mathbf{W}$, respectively, on the assumption that their standard deviations are the same.

The simulation was conducted with $N_p=5$ percent and $N_m=1$ percent. First, we evaluated the perturbation in fault pattern vectors when the noise was present. Similar to experimentally conducting the calibration of the process, a simulation ran when no fixture fault was present. The resulting perturbation bound b_1's for fault pattern vectors on three stations are listed in Table 6. The maximum b_1 for all pattern vectors is 2.83 deg. The value of b_2 is more conservative. Simulation revealed that $\lambda_{\max}(\mathbf{K}_\varepsilon)=0.035$ and $\lambda_{\min}(\mathbf{K}_\varepsilon)=0.001$. Then $b_2=8.04$ deg.

The angles (in degree) between fault pattern vectors at station i are listed as follows, where p, $q=1$, 2, 3, 4, 5, 6. Since these matrices are symmetric, only the upper half is listed.

Table 3 Geometric manifestation of six single faults at the 1st station

Fault	Fault Manifestation	Fault	Fault Manifestation
p=1	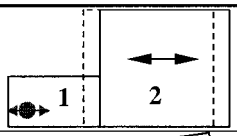	p=4	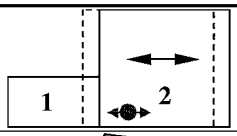
p=2	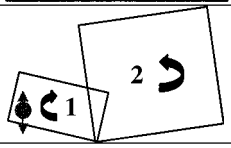	p=5	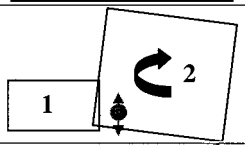
p=3	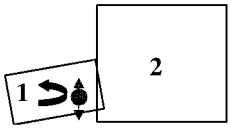	p=6	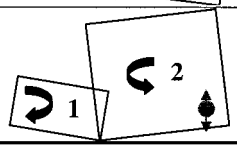

Table 4 Coordinates of locating points in Fig. 3(*b*) (Units: mm)

Tooling	P_1	P_2	P_3	P_4
Position (X, Z)	(100,100)	(580,100)	(800,100)	(1400,100)
Tooling	P_5	P_6	P_7	P_8
Position (X, Z)	(1500,100)	(2000,100)	(2300,100)	(2600,100)

Table 5 Coordinates of sensing points in Fig. 3(*b*) (Units: mm)

Sensors	m_1	m_2	m_3	m_4
Position (X, Z)	(200, 400)	(700, 400)	(700, 600)	(1500, 600)
Sensors	m_5	m_6	m_7	m_8
Position (X, Z)	(1550, 600)	(2100, 600)	(2200, 200)	(2700, 200)

Table 6 Perturbation angle of fault pattern vectors (degree °)

	p=1 or 4	p=2	p=3	p=5	p=6
Station 1	2.47	1.48	2.09	2.38	1.58
Station 2	2.29	1.67	2.83	2.35	1.60
Station 3	2.04	1.97	2.62	1.72	1.91

Table 7 Angle of fault pattern vectors between stations (degree °)

θ(1,2)	θ(2,3)	θ(1,3)
66.2	54.5	76.4

$$[\theta_{pq}(1,1)]=\begin{pmatrix} - & 64.0 & 90 & 0 & 45 & 53.4 \\ & - & 38.3 & 64.0 & 51.7 & 19.3 \\ & & - & 90 & 90 & 57.6 \\ & & & - & 45 & 53.4 \\ & & & & - & 32.4 \\ & & & & & - \end{pmatrix}$$

$$[\theta_{pq}(2,2)]=\begin{pmatrix} - & 53.8 & 90 & 0 & 33.1 & 48.6 \\ & - & 44.9 & 53.8 & 45.1 & 7.27 \\ & & - & 90 & 90 & 52.2 \\ & & & - & 33.1 & 48.6 \\ & & & & - & 37.8 \\ & & & & & - \end{pmatrix}$$

$$[\theta_{pq}(3,3)]=\begin{pmatrix} - & 82.5 & 90 & 0 & 71.1 & 76.7 \\ & - & 23.6 & 82.5 & 66.4 & 21.7 \\ & & - & 90 & 90 & 45.3 \\ & & & - & 71.1 & 76.7 \\ & & & & - & 44.7 \\ & & & & & - \end{pmatrix} \quad (29)$$

It was known that faults of $p=1$ and $p=4$ at each station are identical. Hence the angles between faults $p=1$ and $p=4$ on three stations are zeros. Moreover, the minimum angle formed by the faults of $p=1$ (or 4), 2, 3, 5, 6 is $\theta_{2.6}(2,2)=7.27$ deg, which is the angle between faults $p=2$ and $p=6$ at station 2. This minimum value is larger than $2\times\max(b_1)=5.66$ deg, suggesting that these two fault patterns are still distinct under the current noise level. Hence, the other fault patterns on three stations are also distinguishable by using bound b_1. If bound b_2 is used in the situation that only the eigenvalues of $\mathbf{K}_\varepsilon$ are estimable, then those fixture faults within three stations are still distinguishable, except for the faults of $p=2$ and $p=6$ at station 2 with the angle of 7.27 deg less than $b_2=8.04$ deg, which are not guaranteed distinguishable in the presence of noise.

Similarly, the smallest between-station angles (as defined in Eq. (23)) are given in Table 7. Those values are large enough so that between-station fault patterns are distinct under noise. The large between-station fault angles imply stronger robustness in localizing fixture fault to a certain station, while the smaller in-station angles in Eq. (29) suggest that the isolation of fixture fault within each station is more sensitive to the influence of noise.

Suppose fault $p=6$ occurred at the 1st station. The sample covariance matrix $\mathbf{K}_Y$ is calculated by using 500 samples generated by the VSA [14]. The principal component analysis is performed to get the eigenvalue/eigenvector pairs. The first eigenvalue/eigenvector pair is

$$\lambda_1=0.6011$$

$$\boldsymbol{\gamma}_1=[0.2302\ \ -0.0713\ \ 0.2178\ \ -0.4484\ \ -0.4054\ \ -0.5858\ \ -0.4230\ \ 0.0736\ \ -0.0062\ \ 0.0068\ \ 0.0151\ \ -0.0164\ \ 0.0257\ \ 0.0084\ \ 0.0132\ \ 0.0051]^T \quad (30)$$

The first eigenvalue accounts for 53 percent of the total variation and is 8.5 times larger than the second largest eigenvalue. The angles between $\boldsymbol{\gamma}_1$ and potential fault patterns are listed in Table 8. All units are in degrees.

The smallest angle indicates the fault. Here it is 2.76 deg for $p=6$ at the 1st station. By using within-station fault pattern angles in Eq. (29) and between-station fault pattern angles in Table 7, we know the angle between fault pattern of $p=6$ at station 1 and its closest pattern vector is 19.3 deg, which is larger than $2b_2=16.1$ deg. Thus, the fault is considered to be correctly identified.

5 Conclusions

This paper developed a fixture fault diagnosis method explicitly for multistage manufacturing processes based on product/process design parameters and in-line measurements obtained at the end of production line. The developed state space model was used to describe propagation of fixturing variation throughout production line, and to relate the product quality to fixturing variability. The state space model provided a systematic way to model the set of fault pattern vectors, which are needed for PCA-based pattern recognition. Given the existence of correlated process noises, the upper bound of the perturbation in fixture fault pattern is given by matrix perturbation theory and can be expressed in terms of the eigenvalues of noise covariance matrix. Furthermore, perturbation in fault pattern due to the influence of noise depended on the difference of variances of noises rather than on the absolute values of individual noise variances.

An assembly process was used as an application for the proposed methodology. The single fault patterns of the process, which have a clear geometric interpretation, were obtained from the state space model and interpreted in terms of process/product information. For this specific process, the entire process diagnosability was not ensured because there existed fault patterns either identical or too close to the other fixture fault patterns within a station. However, the between-station fault pattern angles were fairly large, suggesting that the fixture fault could be confidently localized to a certain station based on the end-of-line sensing. Using this process with CAD data from an assembly plant, numerical simulation was conducted to illustrate and verify the method.

Extension of the current work to the diagnosis of multiple simultaneous faults is being investigated by following the concept of observability in control theory. As the total number of stations and involved product components increases, the computation in model development and application could be a burden. It is worthwhile to explore effective ways leading to a reduced model for implementation in practice.

Despite assumptions made for sake of simplicity during the course of modeling and diagnosis, the approach is fairly general for MMPs since it is based on the standard state space model. When more complex variation factors are accommodated in the state space form, the same method can be applied and the analysis will remain valid.

Table 8 Angle between $\boldsymbol{\gamma}_1$ and fault patterns for single fault

	p=1 or 4	p=2	p=3	p=5	p=6
1st station	54.1	18.2	56.4	33.7	**2.76**
2nd station	89.6	84.1	82.3	89.4	84.8
3rd station	88.4	86.0	86.0	89.1	86.6

Acknowledgment

This research is partially supported by The NSF CAREER Award DMI 9624402, NSF Engineering Research Center on Reconfigurable Manufacturing Systems, the University of Wisconsin's Graduate School, and DaimlerChrysler Corporation.

Appendices

Appendix I 3-2-1 Fixture Layout (Fig. 6)

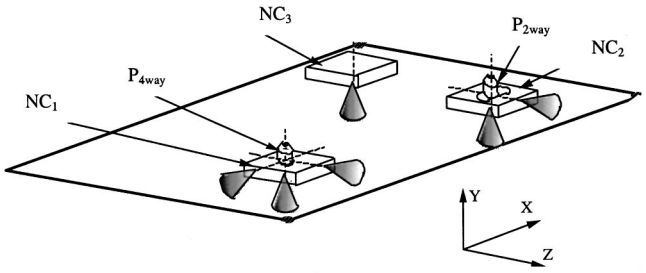

P_{4way}	-	4-way locator controlling part in the X and Z directions
P_{2way}	-	2-way locator controlling part in the Z direction
$NC_{1,2,3}$	-	NC blocks controlling part in the Y direction and rotation

Fig. 6 A layout of 3-2-1 fixture

Appendix II Extension of State Space Model of MMP System Developed in [13]. First, the definition of $\Delta\mathbf{P}(i)$ is expressed as

$$\Delta\mathbf{P}(i)=(\Delta x_{P_1}(i)\ \ \Delta z_{P_1}(i)\ \ \Delta x_{P_2}(i)\ \ \Delta z_{P_2}(i))^T \qquad (a1)$$

This definition differs from that in [13] because this $\Delta\mathbf{P}(i)$ is measured in a global body coordinate system, while $\Delta\mathbf{P}(i)$ in [13] is measured in a local part coordinate system. The modification offers more convenience in using actual measured data since CMM or OCMM readings are based on the global coordinate system. Accordingly, $\mathbf{Q}_{P_1,P_1}(i)$ is changed to

$$\mathbf{Q}_{P_1,P_1}(i)=\begin{bmatrix} 1 & 0 & 0 & 0 \\ 0 & 1 & 0 & 0 \\ \dfrac{\sin\alpha}{L_x(P_1,P_2)} & -\dfrac{\cos\alpha}{L_x(P_1,P_2)} & -\dfrac{\sin\alpha}{L_x(P_1,P_2)} & \dfrac{\cos\alpha}{L_x(P_1,P_2)} \end{bmatrix}_{3\times 4} \qquad (a2)$$

where α is the nominal orientation of a workpiece measured in the global coordinate system. This value cannot be assumed to be small since a workpiece could be positioned at an arbitrary angle.

The modeling assumptions used in [13] can be summarized as

(i) 2-D rigid body part;
(ii) 3-2-1 fixture layout for rigid part;
(iii) Lap joint only so that part fabrication error does not affect variation propagation.
(iv) There are only two workpieces on each station and the second piece should be a single-piece part rather than a multiple-piece subassembly.

The first three assumptions are still kept in the current modeling development. The rigid body assumption is made and 3-2-1 fixture layout is employed as a primary fixture set up. However, the model will also apply to n-2-1 nonrigid body fixturing [23] if the fixture faults being considered cause panel motion only in the plane of rigidity. The simplification of joints used in the assembly model enables us to decouple the stamping variation and the fixturing variation, and thus we can focus on the latter one.

The fourth assumption, however, limits the scope of application of the state space model, and thus model revision is conducted to eliminate it. In order to expand the model to accommodate an assembly process with many workpieces joined at a station, the selecting matrix $\mathbf{W}_1(s)$ is defined as

$$\mathbf{W}_1(s)=[\,\delta_{1s}\mathbf{I}^{4\times4}\ \ \delta_{2s}\mathbf{I}^{4\times4}\ \cdots\ \delta_{ns}\mathbf{I}^{4\times4}]$$

$$\delta_{ks}=\begin{cases}1 & \text{if } k=s\\ 0 & \text{if } k\neq s\end{cases} \text{ is the Kronecker Delta,} \qquad (a3)$$

such that

$$\begin{bmatrix}\Delta\mathbf{P}(i)\\ \Delta\mathbf{P}'(i)\end{bmatrix}=\mathbf{W}_1(s)\mathbf{U}(i), \qquad (a4)$$

where s is the index of the workpiece directly supported by a set of fixture, $\mathbf{U}(i)$ can be multiple sets of fixtures as $\mathbf{U}(i)=[\Delta\mathbf{P}_1(i)\ \Delta\mathbf{P}_2(i)\ \cdots\ \Delta\mathbf{P}_{n_i}(i)]^T$ and $[\Delta\mathbf{P}(i)\ \Delta\mathbf{P}'(i)]^T$ is the $\mathbf{U}(i)$ defined in [13].

Another $\mathbf{W}_2(i)$ is defined to pick up the right reorientation term.

$$\mathbf{W}_2(i)=\begin{bmatrix}\mathbf{w}_{11}^{3\times3} & \mathbf{w}_{12} & \cdots & \mathbf{w}_{1N}\\ \mathbf{w}_{21} & \mathbf{w}_{22} & \cdots & \mathbf{w}_{2N}\end{bmatrix}, \qquad (a5)$$

where

$$\mathbf{w}_{pq}^{3\times3}=\begin{cases}\mathbf{I}^{3\times3} & \text{if } (p,q)=(1,k) \text{ or } (2,j)\\ \mathbf{0}^{3\times3} & \text{otherwise}\end{cases}, \qquad (a6)$$

such that

$$\begin{bmatrix}\mathbf{X}_{A_k}(i)\\ \mathbf{X}_{A_j}(i)\end{bmatrix}=\mathbf{W}_2(i)\mathbf{X}(i), \qquad (a7)$$

where $\mathbf{X}_{A_k}(i)$ and $\mathbf{X}_{A_j}(i)$ are defined in Eq. (22) in [13] and N is the total number of workpieces in the assembly.

Appendix III Theorem 8.1.12 in [21] (p. 399–400). Suppose matrices $\mathbf{S}$ and $\mathbf{S}+\mathbf{E}$ are $n\times n$ symmetric matrices and that $\mathbf{Q}=[\mathbf{q}_1\ \mathbf{Q}_2]$ is an orthogonal matrix such that $\mathbf{q}_1$ is a unit 2-norm eigenvector for $\mathbf{S}$. Partition the matrices $\mathbf{Q}^T\mathbf{S}\mathbf{Q}$ and $\mathbf{Q}^T\mathbf{E}\mathbf{Q}$ as follows

$$\mathbf{Q}^T\mathbf{S}\mathbf{Q}=\begin{bmatrix}\lambda_1 & \mathbf{0}\\ \mathbf{0} & \mathbf{D}_2\end{bmatrix} \text{ and } \mathbf{Q}^T\mathbf{E}\mathbf{Q}=\begin{bmatrix}\delta & \mathbf{e}^T\\ \mathbf{e} & \mathbf{E}_{22}\end{bmatrix}. \qquad (a8)$$

If $d=\min_{\mu\in\lambda(\mathbf{D}_2)}|\lambda_1-\mu|>0$ and $\|\mathbf{E}\|_2\leq d/4$, then the unit 2-norm eigenvector $\hat{\mathbf{q}}_1$ of $\mathbf{S}+\mathbf{E}$ is different from $\mathbf{q}_1$ in such a way that

$$\text{dist}(\text{span}\{\mathbf{q}_1\},\text{span}\{\hat{\mathbf{q}}_1\})=\sqrt{1-(\mathbf{q}_1^T\hat{\mathbf{q}}_1)^2}\leq\frac{4}{d}\|\mathbf{e}\|_2, \qquad (a9)$$

where $\lambda(\mathbf{D}_2)$ is the set of eigenvalues of $\mathbf{D}_2$ and λ_1 is the eigenvalue of $\mathbf{S}$ associated with eigenvector $\mathbf{q}_1$. In this theorem, dist(span $\{\mathbf{q}_1\}$, span $\{\hat{\mathbf{q}}_1\}$) is equal to the sine of the angle between $\mathbf{q}_1$ and $\hat{\mathbf{q}}_1$, i.e., $\Delta\theta_1=\sin^{-1}$ (dist(span $\{\mathbf{q}_1\}$, span $\{\hat{\mathbf{q}}_1\}$)).

Appendix IV Proof of Equation (19). Following Theorem 8.1.12, the upper bound of the angle between $\boldsymbol{\gamma}^0$ and $\boldsymbol{\gamma}$ is

$$\Delta\theta=\sin^{-1}(\text{dist}(\text{span}\{\boldsymbol{\gamma}^0\},\text{span}\{\boldsymbol{\gamma}\})). \qquad (a10)$$

Because $d=\lambda^0$ and $\mathbf{e}=\mathbf{Q}_2^T\mathbf{K}_\varepsilon\boldsymbol{\gamma}^0$, according to Eq. (18),

$$\Delta\theta \leqslant \sin^{-1}\left(\frac{4}{\lambda^0}\|\mathbf{Q}_2^T\mathbf{K}_\varepsilon\boldsymbol{\gamma}^0\|_2\right) = \sin^{-1}\left(\frac{4}{\lambda^0}\sqrt{\boldsymbol{\gamma}^{0T}\mathbf{K}_\varepsilon\mathbf{Q}_2\mathbf{Q}_2^T\mathbf{K}_\varepsilon\boldsymbol{\gamma}^0}\right)$$

Since $\mathbf{Q}_2\mathbf{Q}_2^T + \boldsymbol{\gamma}^0\boldsymbol{\gamma}^{0T} = \mathbf{I}$, then

$$= \sin^{-1}\left(\frac{4}{\lambda^0}\sqrt{\boldsymbol{\gamma}^{0T}\mathbf{K}_\varepsilon(\mathbf{I}-\boldsymbol{\gamma}^0\boldsymbol{\gamma}^{0T})\mathbf{K}_\varepsilon\boldsymbol{\gamma}^0}\right)$$

$$= \sin^{-1}\left(\frac{4}{\lambda^0}\sqrt{\boldsymbol{\gamma}^{0T}\mathbf{K}_\varepsilon\mathbf{K}_\varepsilon\boldsymbol{\gamma}^0 - \boldsymbol{\gamma}^{0T}\mathbf{K}_\varepsilon\boldsymbol{\gamma}^0\cdot\boldsymbol{\gamma}^{0T}\mathbf{K}_\varepsilon\boldsymbol{\gamma}^0}\right)$$

$$= \sin^{-1}\left(\frac{4}{\lambda^0}\sqrt{\|\mathbf{K}_\varepsilon\boldsymbol{\gamma}^0\|_2^2 - (\boldsymbol{\gamma}^{0T}\mathbf{K}_\varepsilon\boldsymbol{\gamma}^0)^2}\right).$$

Notice that $\|\mathbf{K}_\varepsilon\boldsymbol{\gamma}^0\|_2 \leqslant \|\mathbf{K}_\varepsilon\|_2\cdot\|\boldsymbol{\gamma}^0\|_2 = \|\mathbf{K}_\varepsilon\|_2 = \lambda_{\max}(\mathbf{K}_\varepsilon)$ and $\lambda_{\min}(\mathbf{K}_\varepsilon) \leqslant \boldsymbol{\gamma}^{0T}\mathbf{K}_\varepsilon\boldsymbol{\gamma}^0 \leqslant \lambda_{\max}(\mathbf{K}_\varepsilon)$,

$$\therefore \quad \Delta\theta \leqslant \sin^{-1}\left(\frac{4}{\lambda^0}\sqrt{\lambda_{\max}^2(\mathbf{K}_\varepsilon) - \lambda_{\min}^2(\mathbf{K}_\varepsilon)}\right). \qquad (a11)$$

References

[1] Ceglarek, D., and Shi, J., 1995, ''Dimensional Variation Reduction for Automotive Body Assembly,'' Manufacturing Review, **8**, pp. 139–154.

[2] Asada, H., and By, B., 1985, ''Kinematic Analysis of Workpart Fixturing for Flexible Assembly with Automatically Reconfigurable Fixtures,'' IEEE J. Rob. Autom., **RA-1**, pp. 86–94.

[3] Rong, Y., and Bai, Y., 1996, ''Machining Accuracy Analysis for Computer-aided Fixture Design Verification,'' ASME J. Manuf. Sci. Eng., **118**, pp. 289–299.

[4] Choudhuri, S. A., and De Meter, E. C., 1999, ''Tolerance Analysis of Machining Fixture Locators,'' ASME J. Manuf. Sci. Eng., **121**, pp. 273–281.

[5] Ceglarek, D., and Shi, J., 1996, ''Fixture Failure Diagnosis for Auto Body Assembly Using Patter Recognition,'' ASME J. Eng. Ind., **118**, pp. 55–65.

[6] Barton, R. R., and Gonzalez-Barreto, D. R., 1996, ''Process-oriented Basis Representations for Multivariate Process Diagnosis,'' Quality Engineering, **9**, pp. 107–118.

[7] Apley, D. W., and Shi, J., 1998, ''Diagnosis of Multiple Fixture Faults in Panel Assembly,'' ASME J. Manuf. Sci. Eng., **120**, pp. 793–801.

[8] Chang, M., and Gossard, D. C., 1998, ''Computational Method for Diagnosis of Variation-related Assembly Problems,'' Int. J. Prod. Res., **36**, pp. 2985–2995.

[9] Rong, Q., Ceglarek, D., and Shi, J., 2000, ''Dimensional Fault Diagnosis for Compliant Beam Structure Assemblies,'' ASME J. Manuf. Sci. Eng., **122**, pp. 773–780.

[10] Mantripragada, R., and Whitney, D. E., 1999, ''Modeling and Controlling Variation Propagation in Mechanical Assemblies Using State Transition Models,'' IEEE Trans. Rob. Autom., **15**, pp. 124–140.

[11] Lawless, J. F., Mackay, R. J., and Robinson, J. A., 1999, ''Analysis of Variation Transmission in Manufacturing Processes-Part I,'' J. Quality Technol., **31**, pp. 131–142.

[12] Agrawal, R., Lawless, J. F., and Mackay, R. J., 1999, ''Analysis of Variation Transmission in Manufacturing Processes-Part II,'' J. Quality Technol., **31**, pp. 143–154.

[13] Jin, J., and Shi, J., 1999, ''State Space Modeling of Sheet Metal Assembly for Dimensional Control,'' ASME J. Manuf. Sci. Eng., **121**, pp. 756–762.

[14] VSA, 1998, *VSA-3D Release 12.5 User Manual*, Variation System Analysis, Inc., 300 Maple Park Boulevard, St. Clair Shores, MI 48081.

[15] Huang, Q., Zhou, N., and Shi, J., 2000, ''Stream-of-Variation Modeling and Diagnosis of Multi-station Machining Processes,'' *Proceedings of the 2000 ASME International Mechanical Engineering Congress and Exposition*, **MED-11**, pp 81–88.

[16] Callier, F. M., and Desoer, C. A., 1991, *Linear System Theory*, Springer-Verlag, New York.

[17] Kumar, P. R., and Varaiya, P., 1986, *Stochastic Systems: Estimation, Identification and Adaptive Control*, Prentice-Hall, Inc., Englewood Cliffs, NJ 07632.

[18] Johnson, R. A., and Wichern, D. W., 1998, *Applied Multivariate Statistical Analysis*, Prentice-Hall, Upper Saddle River, NJ.

[19] Ceglarek, D., 1994, ''Knowledge-based Diagnosis for Automotive Body Assembly: Methodology and Implementation,'' Ph.D. Dissertation, The University of Michigan, Ann Arbor, MI, 48109.

[20] Ceglarek, D., and Shi, J., 1999, ''Fixture Failure Diagnosis for Sheet Metal Assembly with Consideration of Measurement Noise,'' ASME J. Manuf. Sci. Eng., **121**, pp. 771–777.

[21] Golub, G. H., and Van Loan, C. F., 1996, *Matrix Computations*, 3rd edition, The Johns Hopkins University Press, Baltimore, MD 21218.

[22] Apley, D. W., and Shi, J., 2001, ''A Factor Analysis Method for Diagnosis Variability in Multivariate Manufacturing Processes,'' Technometrics, **43**, pp. 84–95.

[23] Cai, W., Hu, S. J., and Yuan, J. X., 1997, ''Deformable Sheet Metal Fixturing: Principles, Algorithms, and Simulations,'' ASME J. Manuf. Sci. Eng., **118**, pp. 318–324.